



# Experimental Investigation on the Effect of Nickel-plating Thickness on Continuous-wave Laser Welding of Copper and Steel Tab Joints for Battery Manufacturing

Michele Francioso<sup>1</sup> · Caterina Angeloni<sup>1</sup> · Alessandro Fortunato<sup>1</sup> · Erica Liverani<sup>1</sup> · Alessandro Ascari<sup>1</sup>

Accepted: 24 January 2024  
© The Author(s) 2024

## Abstract

The welding of dissimilar materials, such as copper and steel, holds significant industrial significance in the production of electric vehicle batteries. These materials are commonly used in the case of connections between busbars and cylindrical cells inside a battery pack. To optimize welding and guarantee protection against corrosion, nickel is commonly used in the form of a coating. In this paper, the effect of nickel plating thickness on copper-to-steel welds made with laser technology is investigated. The initial phase consists of a statistical characterization of the nickel plating thickness of the busbar in order to identify the thickness ranges. Experiments were conducted using two different fiber laser sources (a single-mode laser source and a beam-shaping laser source) equipped with a Galvo scanner head; the fluence value and the thickness of nickel plating varied during the experiments. The study conducted has revealed that the thickness of nickel plating plays a crucial role in the weld bead interface, particularly when using a single-mode source. Furthermore, when using the beam-shaping laser source, the fluence employed can have a significant impact on both the depth of penetration and the interface width.

---

✉ Michele Francioso  
michele.francioso2@unibo.it

Caterina Angeloni  
caterina.angeloni2@unibo.it

Alessandro Fortunato  
alessandro.fortunato@unibo.it

Erica Liverani  
erica.liverani2@unibo.it

Alessandro Ascari  
a.ascari@unibo.it

<sup>1</sup> Department of Industrial Engineering, Alma Mater Studiorum – University of Bologna, Viale del Risorgimento 2, Bologna 40136, Emilia Romagna, Italy

**Keywords** Laser beam welding · Nickel coating · Copper and steel · Battery manufacturing

## Introduction

With the constant development of electronic devices, vehicles, and energy storage technologies, the efficiency and reliability of lithium-ion batteries (LIBs) have become critical to ensuring optimal performance [3].

The internal structure of a battery is made up of several cells that, when linked together efficiently, form a module and ultimately a pack, ensuring a reliable and continuous supply of energy. In this context, connections between the cells play a critical role in certifying the stability, life, and efficiency of the battery.

Cells need to be connected in a parallel or series configuration for current to flow and energy to be efficiently transmitted, preventing losses or performance issues.

For individual cylindrical cells, the casings are typically made of aluminum [2], an electro nickel-plated diffusion annealed strip steel, due to its excellent formability and consistent mechanical properties. Weld joints in EV battery packs involve low-thickness materials (typically 0.3 mm to 1 mm), and the welding process is normally performed in a lap joint configuration [5].

A typical joint between steel and Cu busbar is done through fusion welding techniques such as laser beam welding (LBW), micro-spot welding, and ultrasonic welding and is often referred to as “tab welding” [8].

Nowadays, LBW technology is the most popular thanks to its production speeds and accuracy. It is challenging to achieve a complete metallurgical connection without significant cracks and porosities because dissimilar materials have different thermo-physical properties, such as melting temperature and heat conductivity [6].

The tab's material is chosen based on a variety of factors, but the most crucial is electrical and thermal conductivity while still being lightweight and cost-effective. Because of its excellent electrical characteristics and ability to create a robust metallurgical bond with steel while creating a limited quantity of intermetallic phases, copper is the material of choice for busbar tabs.

However, copper-steel joints without a coating layer are prone to corrosion. To mitigate this problem, a layer of nickel is applied to both materials, protecting the joint from corrosive attack. Nickel also increases the absorptivity of the laser and makes welding more efficient.

Electroplating (or electrolytic coating) is a process by which a layer of nickel is deposited on a metal surface through the application of an electric current. The piece to be plated is immersed in an electrolytic solution containing nickel salts dissolved in water. The workpiece to be plated serves as the cathode, while a nickel anode or rod of inert material (such as platinum) serves as the nickel source. By applying an electric current between the anode and the cathode, the nickel ions in the solution are reduced and deposited on the surface of the workpiece, forming a metallic nickel layer.

The electroplating process is complex; the difficulty of the process arises from the involvement of numerous parameters, which pose challenges in maintaining a uniform thickness of nickel plating.

In the e-mobility sector, the use of busbars with a non-uniform nickel-plating thickness could cause differences in terms of electrical resistance, mechanical resistance, and geometric aspect between the busbar-cell joints made by laser welding.

A difference in the physical properties of the joints within a battery module is not desirable as it can create imbalances in the battery's operation during its use. Inconsistencies in connection resistance within battery modules contribute greatly to an overall variation of the parameters and, finally, to the uneven aging of the individual cells. Therefore, from a production point of view, a requirement for a joining technique is that a narrow dispersion range of the resulting connection resistance is obtainable [8].

LBW could have several defects impacting the system's efficiency and safety in battery pack manufacturing.

Among the most common defects it's possible to identify porosities, caused by trapped gas in the welding bead [1], and incomplete fusion, which leads to weakly bonded joints.

Further defects include spatter, or molten metal particles expelled from the melting pool [7], and cracks developing when the metal solidifies.

In the literature on laser welding joints, it is difficult to find sources on the impact of nickel-plating thickness. It's important to study its effect in cell-to-busbar welds for developing zero-defect processes in the automotive sector; therefore, this document aims to provide a first study regarding the influence of plating thickness on the geometric qualities of the weld seams produced by laser technology. In the following sections, the methodologies used to carry out the experimentation will be summarized, and the results will be analyzed using statistical methods.

## Materials and Methods

The purpose of the experimental campaign is to investigate the influence of the nickel-plating thickness on joints obtained by laser beam welding, by varying the process parameters and the type of source used.

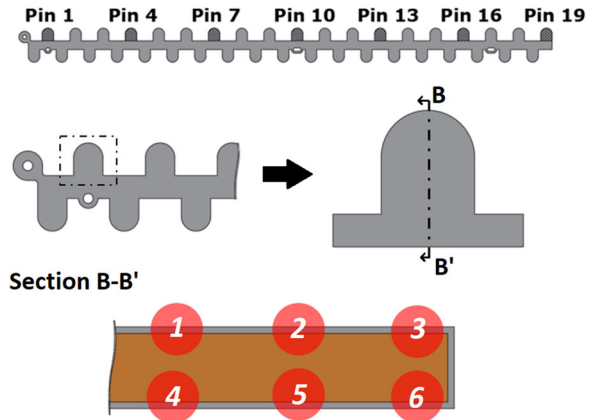
Our procedure was to first identify areas with different thicknesses of nickel plating inside the busbar, and then carry out the experiments.

### Nickel Thickness Measurements

The busbar consists of a main section with pins that serve as connection areas for the batteries. The nominal thickness of the busbar is 0.4 mm. The busbar is made of copper alloys (C11000) and nickel-plated through an electrolytic process, with a nominal thickness of nickel plating of 7  $\mu\text{m}$ . Three randomly chosen busbars from the entire set were analyzed in order to determine the real thickness of the nickel plating. The geometry of the busbars is shown in Fig. 1.

The thicknesses of pins 1, 4, 7, 10, 13, 16, and 19 for each busbar have been investigated. To measure the nickel-plating thickness, each pin was sectioned, embedded, polished, and inspected under a microscope. The detailed procedure has been described in the "[Metallographic Procedure](#)".

**Fig. 1** Busbar geometry and section view for nickel thickness measurements



It was feasible to obtain six different measurements for each pin by fragmenting it into six zones (Fig. 1): three superior zones and three bottom zones.

The one-way ANOVA (Analysis of Variance) is a statistical method used to describe the thickness of the nickel plating on the busbar. In a one-way ANOVA, the means of two or more groups are compared for a single dependent variable. When the investigation involves more than two groups, a one-way ANOVA is necessary [4].

The groups in the analysis are the busbar pins, and the associated nickel-plating thickness is the dependent variable.

The study used Minitab to carry out the ANOVA analysis.

## Laser Welding

In order to investigate the impact of nickel-plating thickness on weld quality and geometry, a replication of the industrial process set up to manufacture a battery module has been made.

It used "dummy" type 21700 cylindrical cells made of Ni-coated diffusion annealed steel (Hilumin) to carry out the experiment. Each cylindrical cell was 21 mm in diameter, 70 mm long, and had a case thickness of 0.5 mm on the positive pole and 0.3 mm on the negative pole.

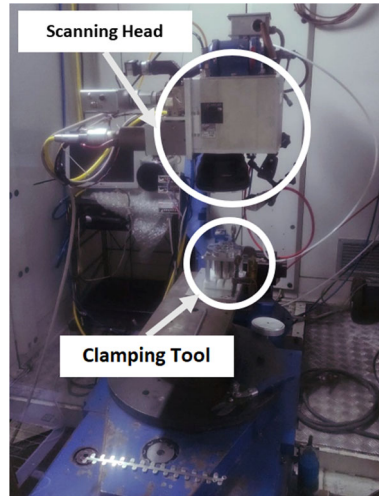
Continuous wave (CW) welding in an overlapping configuration between the busbar and the positive pole of the cylindrical cell (type 21700) was used to create the straight-line shape 4mm long.

A specially designed clamping tool was utilized to ensure that there was zero gap between the busbar and the positive pole. Before the welding process, the samples were thoroughly cleaned with acetone solutions.

The experiment was carried out using two near-infrared (1064 nm) laser sources: A single mode n-light ALTA 1200 SM and a beam shaping n-light CORONA CFX5000 source. CORONA CFX5000 source was used in Index 0 (100% Power in the core).

The optical scheme used consisted of a collimating lens, a scanner head, and an f-theta focusing lens. For the single-mode laser source, an *SCANLAB INTELLISCAN20*

Fig. 2 Experimental Setup



head with an f-theta lens with a 255 mm focal length was utilized and a resulting theoretical spot diameter of  $49 \mu\text{m}$  was obtained.

The scanner head utilized for the corona source was a *SCANLAB HURRYSCAM30* with a 163 mm f-theta lens, and a final spot of  $180 \mu\text{m}$  was calculated.

To facilitate movement of the optics within the welding area, the Galvo scanner head was mounted on a 6-axis anthropomorphic robot (Yaskawa-Motoman HP-20).

Before welding, the head was moved, using the robot, onto the cell to be welded. During the welding process, the robot remained stationary, and the movement of the beam was executed by the galvos. No shielding gas was used, and a high-pressure lateral air jet was employed to protect the scanning optics. The laser beam was directed onto the surface of the top sheet without tilting the head.

In Fig. 2, the experimental setup is shown and the details of the sources and focusing systems are given in the Table 1.

Table 1 Laser sources properties

		ALTA 1200 SM	CORONA CFX5000
Beam's wavelength	[nm]	1064	1064
Operative Method		CW	CW
Max Laser Power	[W]	1200	5000
BPP	[mm · mrad]	0.4	3.1
Collimation length	[mm]	120	80
Focal Length	[mm]	255	163
Fiber Diameter	[ $\mu\text{m}$ ]	14	90
Spot Diameter	[ $\mu\text{m}$ ]	49	180

Laser Irradiance (defined as the ratio between power and spot area) was constant for each laser source, while Fluence (defined as the product between irradiance and interaction time) varied.

Specific equations for Fluence (Eq. 1) and interaction time ( $\tau$ ) (Eq. 2) are the following:

$$F = \frac{P\tau}{A} \quad \left[ \frac{\text{J}}{\text{mm}^2} \right] \quad (1)$$

$$\tau = \frac{L}{v} \quad [\text{s}] \quad (2)$$

where  $P$  is the Power of the laser source [W],  $A$  is the laser spot area [ $\text{mm}^2$ ],  $L$  is the length of the trace [mm],  $v$  is the speed of the laser beam [mm/s].

The experimental tests were carried out with both sources for the two levels of nickel-plating thickness and by varying the Fluence.

The thickness levels for nickel plating are explained in “[Busbar Characterization](#)”, which also examines its evolution along the busbar. Table 5 shows two zones: a lower-level zone with an average nickel plating thickness of  $8.9 \mu\text{m}$  and a high-level zone with an average nickel plating thickness of  $30.3 \mu\text{m}$ .

In the experiments carried out with the single-mode laser source, the Fluence value is between  $6363 \text{ J/mm}^2$  and  $4242 \text{ J/mm}^2$ , while for the tests carried out with the beam-shaping laser source, the Fluence value is between  $1257 \text{ J/mm}^2$  and  $1028 \text{ J/mm}^2$ .

The Fluence values were chosen from an earlier optimization that aimed to identify the operating window for the analysis.

The laser power was defined as a constant, specifically equal to 600 W for the tests carried out with the single-mode source (n-light ALTA 1200 SM) and 1800 W for the tests carried out with the beam-shaped laser source (n-light CORONA CFX5000). The speeds have been chosen in ranges between 200 mm/s and 300 mm/s in order to guarantee the production rate.

A mixed-level factorial design was created using as factors the speed of the laser (and therefore the associated Fluence) and the level of nickel-plating thickness. The laser speed was varied on 3 levels while the thickness zone was on 2 levels.

Each trial was repeated three times. Table 2 contains details on the welding parameters.

## Metallographic Procedure

To conduct metallographic examinations, the weld samples were cut in half perpendicular to the weld line using abrasive cutters and then mounted in resin (Fig. 3). The specimens were then ground with SiC paper ranging from 80 to 2500-grit, and polished with  $1 \mu\text{m}$  alumina suspension solutions. A solution of 2% Nital etchant was used to identify the weld seam geometry.

The geometry of the weld beads cross-section was studied using a Zeiss Observer A1M optical microscope. Once acquired, the penetration depth into the lower sheet can be measured from the interface between the two materials. Similarly, the interface width of the weld can be measured at the joint between the two sheets.

**Table 2** Welding parameters

Source	ID	Laser Velocity [mm/s]	Thickness Zone	Fluence [J/mm <sup>2</sup> ]
n-light ALTA 1200 SM	1.1	200	HIGH	6363
	1.2	250	HIGH	5090
	1.3	300	HIGH	4242
	2.1	200	LOW	6363
	2.2	250	LOW	5090
	2.3	300	LOW	4242
n-light CORONA CFX5000	3.1	225	HIGH	1257
	3.2	250	HIGH	1131
	3.3	275	HIGH	1028
	4.1	225	LOW	1257
	4.2	250	LOW	1131
	4.3	275	LOW	1028

After collecting the morphological data of the welding sections, the aspect ratio index was calculated for each weld seam using the following formula:

$$A_r = \frac{\text{Seam Depth}}{\text{Width}} \quad (3)$$

Geometric results were then correlated with process parameters and nickel-plating thickness.

## Results and Discussion

### Busbar Characterization

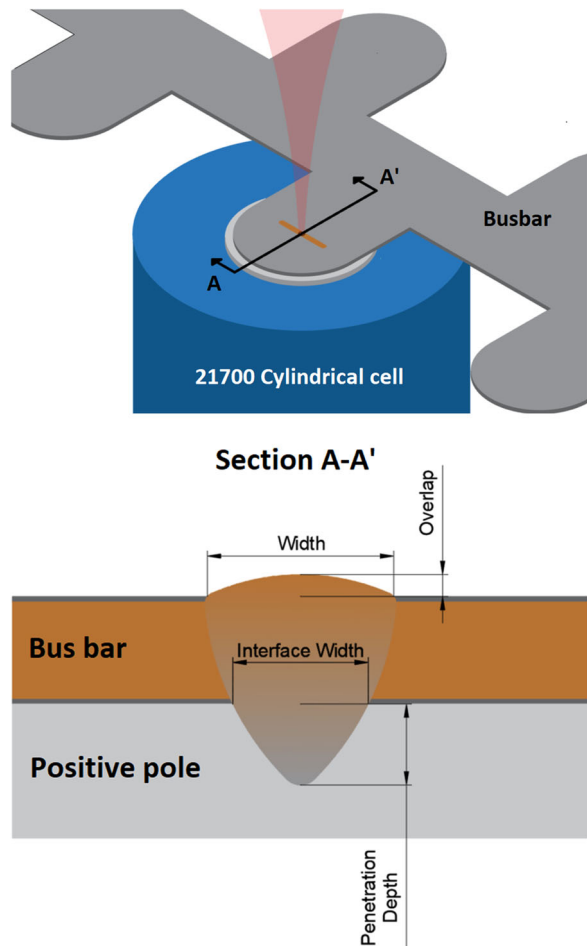
Table 3 displays the results obtained from the analysis of variance (ANOVA). A one-way ANOVA revealed that there was a statistically significant difference in the thickness of the nickel plating along the busbar pins between at least two groups (F-value = 46.90, P-value < 0.001).

Tukey's HSD Test for multiple comparisons (Table 4) found that the mean value of nickel-plating thickness was significantly different between three different groups of pins as shown in the table.

Consequently, we can categorize the nickel-plating thickness into three different groups (Table 5): low, medium, and high thickness groups.

Figure 4 displays how the thickness of the nickel plating changes varying the pins.

**Fig. 3** Process representation and weld seam characteristics



### Welding Characterization

The microscope images of the welded specimens obtained with the Single mode Laser source are presented in Fig. 5. Table 6 shows the average measurements of the main geometric characteristics of the weld seams.

Figure 6 illustrates the penetration depth trends and the interface width trends as a function of Fluence and the nickel-plating thickness level.

**Table 3** One-way ANOVA resume table for Busbar characterization

Source	DF	Adj SS	Adj MS	F-Value	P-Value
PIN	6	7186	1197.64	46.90	0.000
Error	119	3039	25.53		
Total	125	10224			

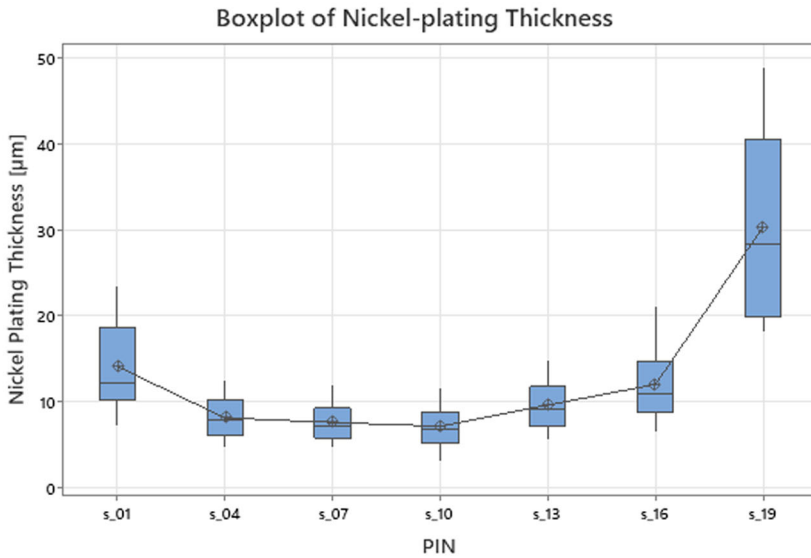


**Table 4** Grouping Information Using the Tukey Method and 95% Confidence

PIN	N	Mean [ $\mu\text{m}$ ]	Grouping	
19	18	30.3	A	
01	18	14.1	B	
16	18	12.0	B	C
13	18	9.7	B	
04	18	8.2	C	
07	18	7.6	C	
10	18	7.2	C	

**Table 5** Clustering table of busbar

Group	PIN	Nickel Thickness mean value [ $\mu\text{m}$ ]
Low	From 04 to 16	8.9
Medium	From 01 to 03	14.1
High	From 17 to 19	30.3

**Fig. 4** Nickel plating thickness trend graph

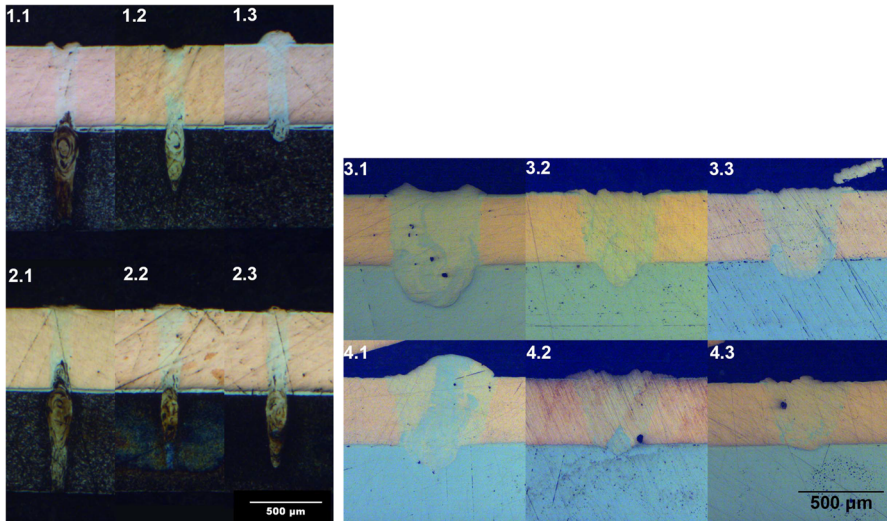


**Fig. 5** Microscope Image of welded specimen

Considering the penetration depth and the interface width as responses, two factorial analyzes were performed for each source used, using the Fluence and the nickel-plating thickness levels of the busbar as factors. The results of the factorial analyzes relating to the tests carried out with the single-mode source can be observed in the Tables 7 and 8. Using the penetration depth as a response, we did not find a statistically significant difference by varying the Fluence (F-value = 1.81, P-value = 0.205) and the nickel-plating thickness (F-value = 1.30, P-value= 0.277) as parameters, and the interaction between these terms was not significant (F-value = 0.56, P-value = 0.588).

**Table 6** Average measurements of the main geometric characteristics of the weld seams

ID	Penetration Depth [ $\mu\text{m}$ ]	Interface Width [ $\mu\text{m}$ ]	Width [ $\mu\text{m}$ ]	Overlap [ $\mu\text{m}$ ]	Depth [ $\mu\text{m}$ ]	Aspect Ratio
1.1	396	95	99	15	796	8.04
1.2	362	113	116	22	762	6.57
1.3	350	93	95	23	751	7.90
2.1	494	88	92	13	894	9.72
2.2	422	91	94	17	822	8.74
2.3	340	80	84	20	740	8.81
3.1	194	457	591	49	594	1.00
3.2	142	327	557	42	542	1.04
3.3	76	266	435	58	476	0.92
4.1	142	367	590	96	542	1.09
4.2	95	314	527	64	495	1.07
4.3	74	262	524	39	474	1.11

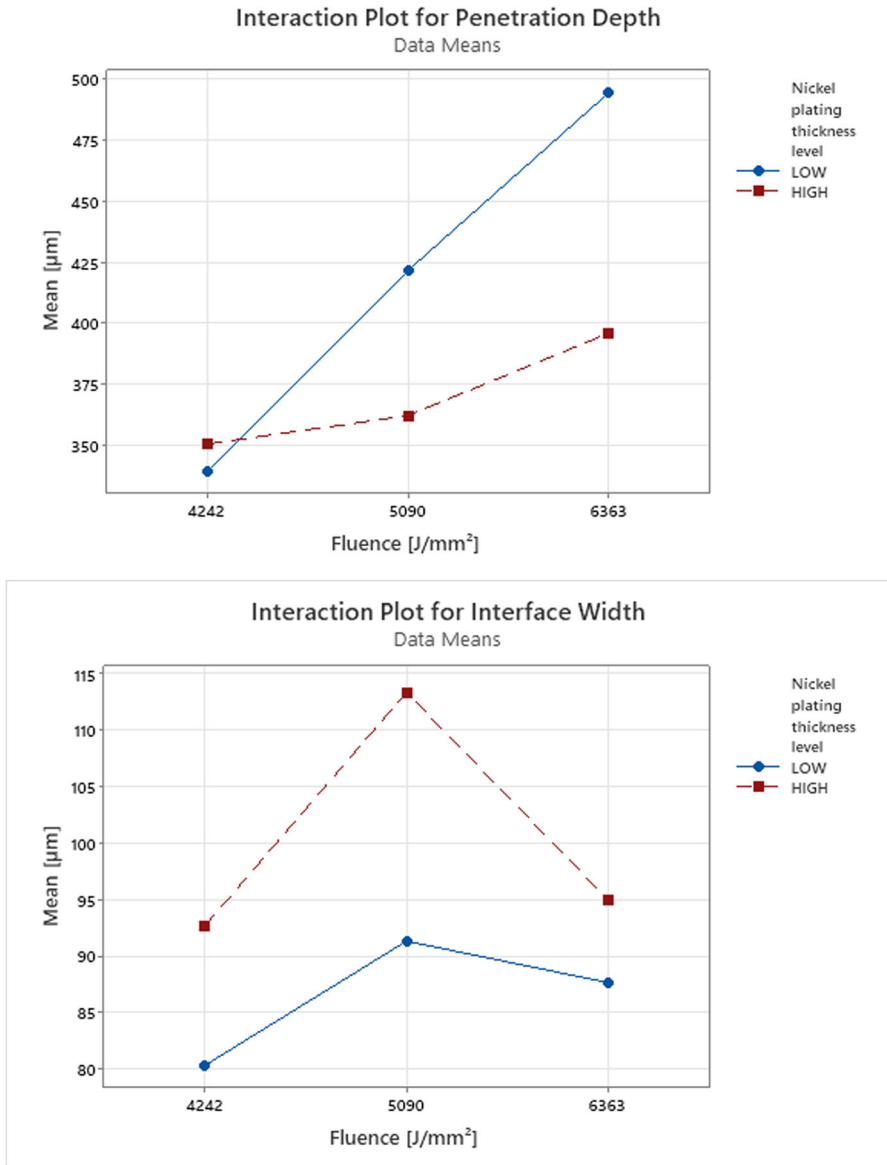


**Fig. 6** Penetration depth trends and interface width trends varying Fluence and Nickel-plating Thickness level for single-mode trial

However, setting the interface width as a response, we find a statistically significant difference by varying the nickel-plating thickness (F-value = 6.07, P-value= 0.030) but no statistical difference varying the Fluence (F-value = 2.76, P-value = 0.103) and the interaction between these terms (F-value = 0.58, p-value= 0.573).

**Table 7** Analysis of Variance - Single mode Source (Penetration Depth)

Source	DF	Adj SS	Adj MS	F-Value	P-Value
Model	5	50006	10001	1.21	0.364
Linear	3	40796	13599	1.64	0.233
Fluence	2	30040	15020	1.81	0.205
Nickel plating thickness level	1	10756	10756	1.30	0.277
2-Way Interactions	2	9211	4605	0.56	0.588
Fluence*Nickel plating thickness level	2	9211	4605	0.56	0.588
Error	12	99541	8295		
Total	17	149548			

It is therefore possible to state that at the interface, the nickel-plating thickness is a statistically significant variable, the result being that as the nickel-plating thickness increases, the width at the interface increases.

The standardized effect Pareto chart for the penetration depth and interface width of the trial made with the single mode laser source are shown in the Fig. 8.

Microscope images of welded specimens obtained with the Corona Laser source are shown in Fig. 5. Related to it, the average measurements of the main geometric characteristics of the weld seams can be viewed in Table 6. Figure 7 shows the penetration depth trends and the interface width trends as a function of Fluence and the nickel-plating thickness level.

The results of the factorial analyzes relating to the tests carried out with the beam-shaping source can be observed in the Tables 9 and 10. Using the penetration depth as a response, we find a statistically significant difference by varying the Fluence (F-value = 10.15, P-value = 0.003) but no statistical difference by varying the nickel-plating thickness level (F-value = 4.03, P-value = 0.068) and the interaction between these terms (F-value = 0.88, P-value = 0.440).

The same results were obtained by analyzing the interface width as a response, a statistical difference was found by varying the Fluence (F-value = 14.92, P-value = 0.001) and no statistically significant difference by varying the level of nickel-plating

**Table 8** Analysis of Variance - Single mode Source (Interface Width)

Source	DF	Adj SS	Adj MS	F-Value	P-Value
Model	5	1824.9	364.99	2.55	0.085
Linear	3	1658.2	552.72	3.86	0.038
Fluence	2	790.1	395.06	2.76	0.103
Nickel plating thickness level	1	868.1	868.06	6.07	0.030
2-Way Interactions	2	166.8	83.39	0.58	0.573
Fluence*Nickel plating thickness level	2	166.8	83.39	0.58	0.573
Error	12	1717.3	143.11		
Total	17	3542.3			

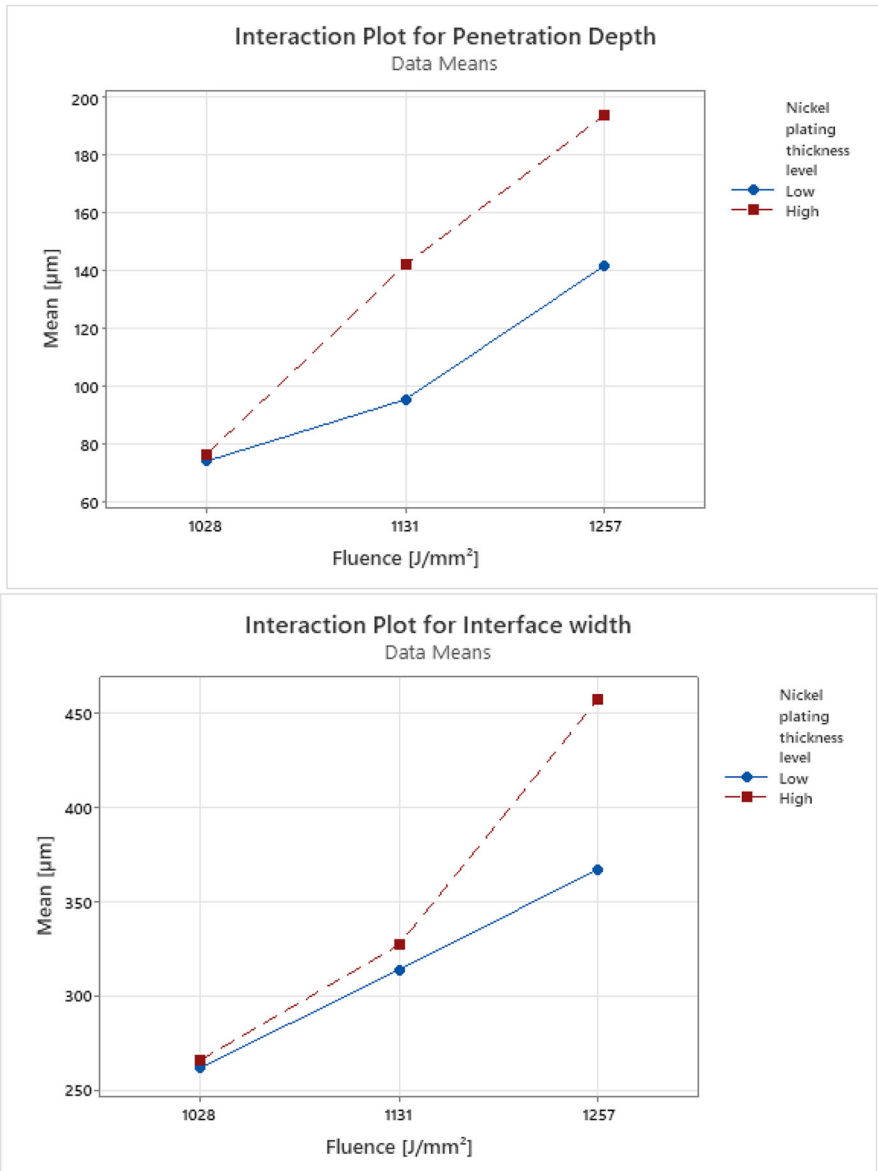


**Fig. 7** Penetration depth trends and interface width trends varying Fluence and Nickel-plating Thickness level for beam-shaping trial

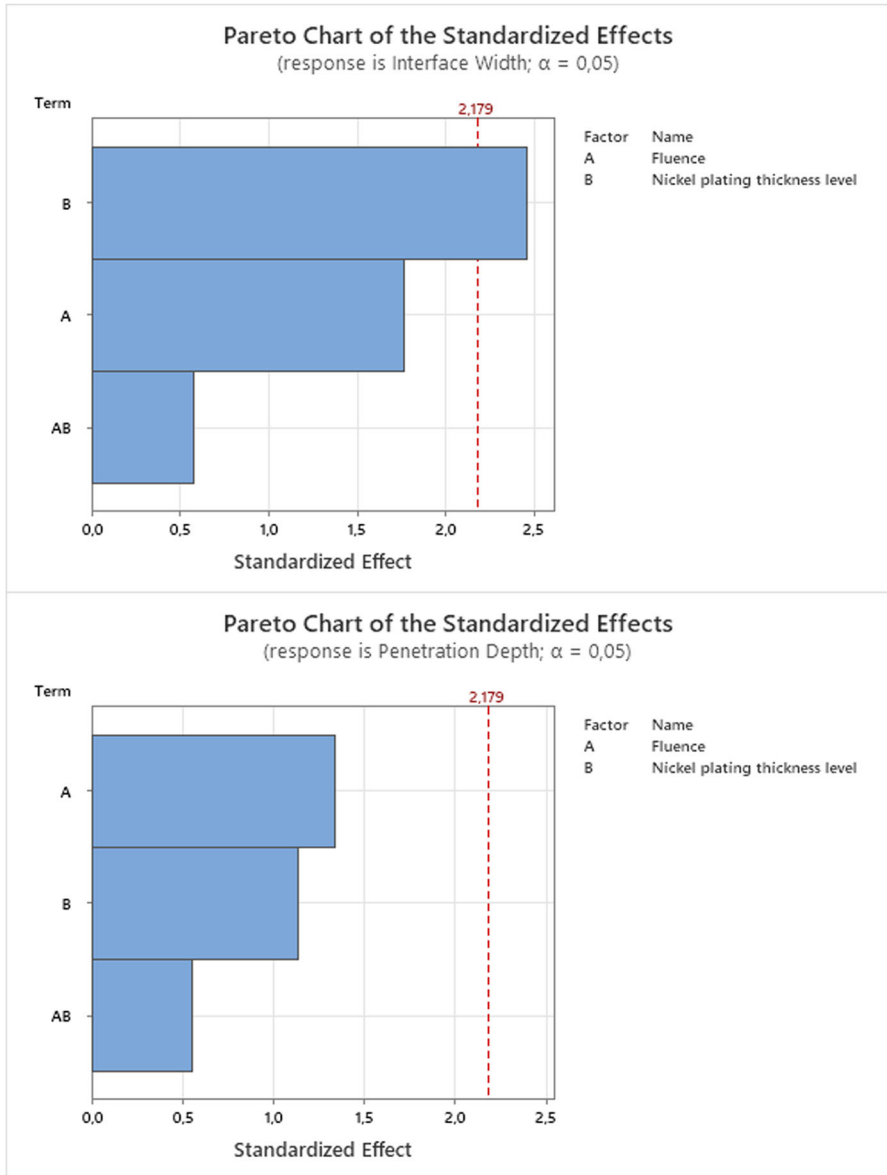


**Fig. 8** Standardized effect Pareto chart for the penetration depth and interface width of the trial made with the single-mode laser source

**Table 9** Analysis of Variance - Beam-shaping laser Source (Penetration Depth)

Source	DF	Adj SS	Adj MS	F-Value	P-Value
Model	5	33030	6606	5.22	0.009
Linear	3	30799	10266	8.11	0.003
Fluence	2	25699	12849	10.15	0.003
Nickel plating thickness level	1	5101	5101	4.03	0.068
2-Way Interactions	2	2230	1115	0.88	0.440
Fluence*Nickel plating thickness level	2	2230	1115	0.88	0.440
Error	12	15199	1267		
Total	17	48229			

thickness (F-value = 3.87, P-value = 0.073) and the interaction between them (F-value = 1.99, P-value = 0.179).

The standardized effect Pareto chart for the penetration depth and interface width of the trial made with the beam-shaping laser source are shown in the Fig. 9. It can be stated that with the use of this laser source, the effect of Fluence on the geometric characteristics of the weld bead is statistically more influential than the level of the nickel-plating thickness.

The results revealed disparities in aspect ratios, with high values associated with the single-mode source and low values with the beam-shaping laser source. The single-mode laser source is characterized by a highly focused beam, which allows for greater precision in the concentration of energy in a specific area and a greater energy density. Therefore, a single-mode laser source produces beads with a high aspect ratio, expressed into beads with low width values at the interface.

On the other hand, the beam-shaping laser source distributes the energy more diffusely, generating weld seams with lower aspect ratio values, represented as seams with higher interface width values compared to the seams obtained with the single mode source.”

**Table 10** Analysis of Variance - Beam-shaping laser Source (Interface Width)

Source	DF	Adj SS	Adj MS	F-Value	P-Value
Model	5	4E+10	8.01E+09	7.54	0.002
Linear	3	3.58E+10	1.19E+10	11.24	0.001
Fluence	2	3.17E+10	1.58E+10	14.92	0.001
Nickel plating thickness level	1	4.11E+09	4.11E+09	3.87	0.073
2-Way Interactions	2	4.24E+09	2.12E+09	1.99	0.179
Fluence*Nickel plating thickness level	2	4.24E+09	2.12E+09	1.99	0.179
Error	12	1.27E+10	1.06E+09		
Total	17	5.28E+10			

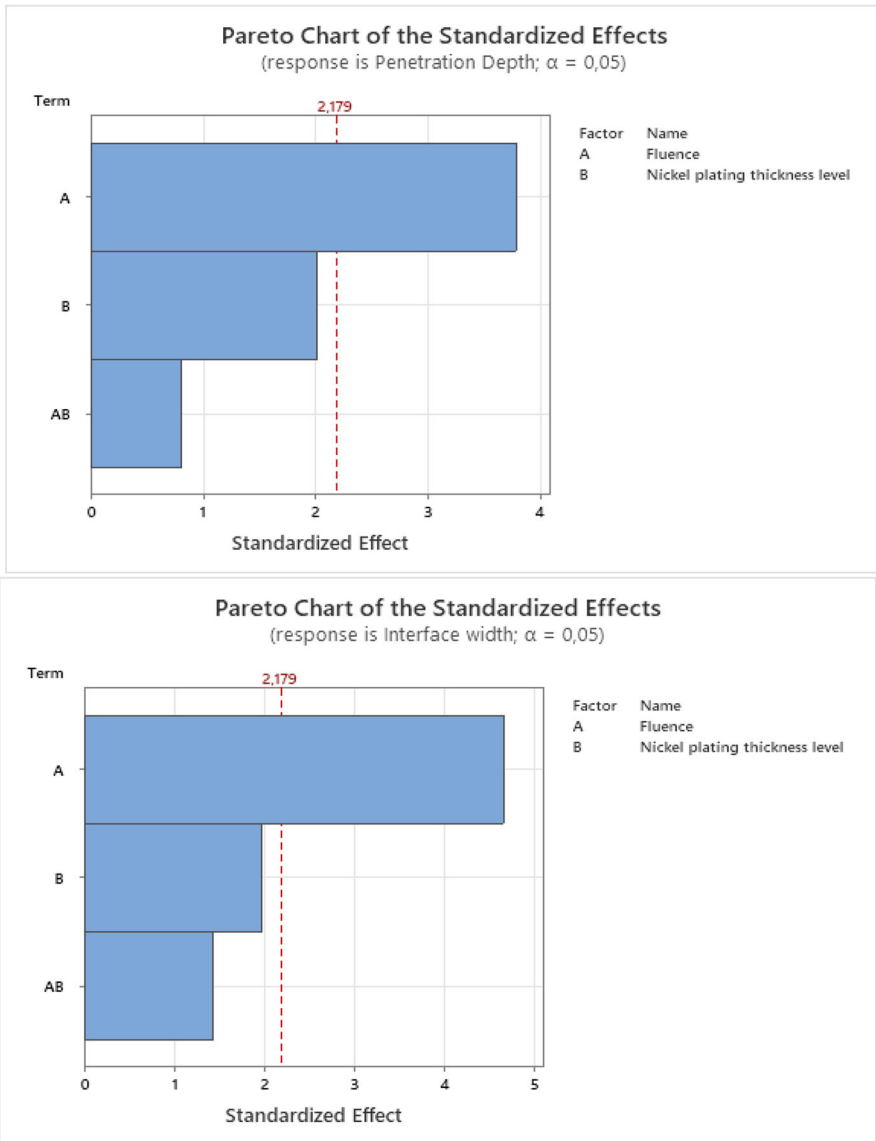


**Fig. 9** Standardized effect Pareto chart for the penetration depth and interface width of the trial made with the beam-shaping laser source

## Conclusion

This research study examines the impact of variations in nickel plating thickness on the laser welding of copper busbars (C11000 alloy) that are coated with electrolytic nickel plating and 21700 dummy cells composed of hilumin.

The results of the study are summarized as follows:



- The factorial analysis of the tests carried out with the single-mode source showed that the weld interface width is influenced by the thickness of the nickel plating;
- The factorial analysis of tests using the beam-shaping source indicated that only the Fluence is statistically significant for weld beads shape;

The width at the interface is a main feature of a busbar-cell joint; its value directly influences the electrical resistance of the joint; therefore, future analyses will focus on studying more deeply the relationship between nickel plating thickness and interface width of joints made with single-mode laser sources.

**Acknowledgements** *Optoprim Italia S.r.l. a socio unico* provided both laser sources.

**Author Contributions** Michele Francioso: Conceptualization, Investigation, Measurement and writing. Angeloni Caterina: Investigation. Alessandro Fortunato, Erica Liverani and Alessandro Ascari: Supervision and manuscript review.

**Funding** Open access funding provided by Alma Mater Studiorum - Università di Bologna within the CRUI-CARE Agreement.

## Declarations

**Competing interests** The authors declare no competing interests

**Open Access** This article is licensed under a Creative Commons Attribution 4.0 International License, which permits use, sharing, adaptation, distribution and reproduction in any medium or format, as long as you give appropriate credit to the original author(s) and the source, provide a link to the Creative Commons licence, and indicate if changes were made. The images or other third party material in this article are included in the article's Creative Commons licence, unless indicated otherwise in a credit line to the material. If material is not included in the article's Creative Commons licence and your intended use is not permitted by statutory regulation or exceeds the permitted use, you will need to obtain permission directly from the copyright holder. To view a copy of this licence, visit <http://creativecommons.org/licenses/by/4.0/>.

## References

1. Matsunawa, A., Mizutani, S.K.M., Seto, N.: Porosity formation mechanism and its prevention in laser welding. *Weld. Int.* **17**(6), 431–437 (2003). <https://doi.org/10.1533/wint.2003.3138>
2. Anon.: Tata steel, “hilumin” tata steel in Europe. <https://www.tatasteeleurope.com/engineering/products/electro-plated/hilumin-ultra-clean-nickel-plated-steel> (2023). Accessed 12 Aug 2023
3. Lai, X., Chen, Q., Tang, X., et al.: Critical review of life cycle assessment of lithium-ion batteries for electric vehicles: A lifespan perspective. *eTransportation* **12** (2022). <https://doi.org/10.1016/j.etrans.2022.100169>
4. Ross, A., Willson, V.L.: One-Way Anova, SensePublishers, Rotterdam, pp. 21–24 (2017). [https://doi.org/10.1007/978-94-6351-086-8\\_5](https://doi.org/10.1007/978-94-6351-086-8_5)
5. Sadeghian, A., Iqbal, N.: A review on dissimilar laser welding of steel-copper, steel-aluminum, aluminum-copper, and steel-nickel for electric vehicle battery manufacturing. *Opt. Laser Technol.* **146**, 107595 (2022). <https://doi.org/10.1016/j.optlastec.2021.107595>. <https://www.sciencedirect.com/science/article/pii/S0030399221006836>
6. Trinh, L.N., Lee, D.: The characteristics of laser welding of a thin aluminum tab and steel battery case for lithium-ion battery. *Metals* **10**(6) (2020). <https://doi.org/10.3390/met10060842>. <https://www.mdpi.com/2075-4701/10/6/842>
7. Zhang, M., Chen, G., Zhou, Y., et al.: Observation of spatter formation mechanisms in high-power fiber laser welding of thick plate. *Appl. Surf. Sci.* **280**, 868–875 (2013). <https://doi.org/10.1016/j.apsusc.2013.05.081>. <https://www.sciencedirect.com/science/article/pii/S0169433213010088>

8. Zwicker, M., Moghadam, M., Zhang, W., et al.: Automotive battery pack manufacturing – a review of battery to tab joining. *J. Adv. Join. Process.* **1**, 100017 (2020). <https://doi.org/10.1016/j.jajp.2020.100017>. <https://www.sciencedirect.com/science/article/pii/S2666330920300157>

**Publisher's Note** Springer Nature remains neutral with regard to jurisdictional claims in published maps and institutional affiliations.